



The effects of PEG molecular weight on fused silica glass sintering by using nano silicon oxide powder

Youwang Hu¹ · Qinglong Zhang¹ · Yaowei Feng¹ · Changsheng Wan¹ · Xiaoyan Sun¹ · Ji'an Duan¹

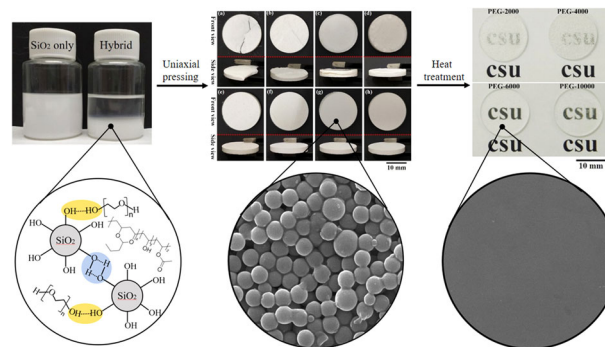
Received: 25 June 2022 / Accepted: 4 October 2022 / Published online: 23 October 2022

© The Author(s), under exclusive licence to Springer Science+Business Media, LLC, part of Springer Nature 2022

Abstract

Sintering pressed nanocomposites to obtain fused silica glasses was a simple and efficient method, while the binder plays an essential role in this process. This paper studied the influence of binder polyethylene glycol (PEG) with different molecular weights on sintering quality. The pH, viscosity, and thermal analysis of nanocomposites were analyzed. PEG of different molecular weights affects the size r of aggregated silica particles by influencing the viscosity of the suspension system and the interaction f of PEG-SiO₂, which affects the specific heat capacity (C_p) and initial fusing temperature (T_i) finally. It was found that the pressed part with PEG-6000 could be densified completely after vacuum sintering for 30 min, comparing the optical images and SEM images. However, the rest pressed parts to have suboptimal optical quality since seam defects. The sintering quality of pressed parts was closely related to the trend of initial fusing temperature T_i with PEG molecular weight, and in the event of lower temperature T_i , the better sintering quality.

Graphical abstract



Keywords Silica glass · PEG molecular weight · Silica nanopowder · Sintering

Highlights

- Transparent fused silica glass was prepared with the binder of PEG and PVB.
- PEG molecular weights affect the quality of sintered parts owing to the suspension viscosity as well as the specific heat capacity (C_p) and initial fusing temperature (T_i) with different.
- The PEG-6000 has the best performance according to the optical and sintering quality.

✉ Xiaoyan Sun
sunxy@csu.edu.cn

¹ State Key Laboratory of High-Performance Complex Manufacturing, College of Mechanical and Electrical Engineering, Central South University, Changsha 410083, China

1 Introduction

Fused silica glasses are widely used in the fields of optics, electronics, and chemical manufacturing because of their extraordinary physicochemical properties, including high

transparency, low thermal expansion coefficient, long-term chemical durability, good electrical insulation, and high hardness [1–4]. Conventionally, the fused silica glasses that are manufactured often require a higher temperature to be melted (temperatures from 2000 to 2300 K) [5] or need extreme conditions of corrosive, toxic, and dangerous solutions such as hydrofluoric acid, ammonium fluoride, and sodium hydroxide [6], which incurs high costs due to environment-hazardous, significant energy losses, and strict equipment requirements. In order to solve these problems, researchers have developed gel-casting [7–9], compression molding [1], powder injection molding [3, 10], three-dimensional printing [11, 12], and other molding methods by taking advantage of the high surface energy property in nano-silica powder. The molded sample can be sintered to be transparent glass components with a density of 2.2 g/cm^3 at a lower temperature of $\sim 1300 \text{ }^\circ\text{C}$.

The fabrication of transparent glass from silica powder to bulk glasses needs to use polymer organic matter to improve the molding properties of materials (rheological properties, structural strength, etc.). Organic compounds can be divided into dispersant (polyvinyl pyrrolidone, stearic acid), binder (polyethylene glycol (PEG), low-density polyethylene, polypropylene), and sturdy skeleton materials (polyvinyl alcohol, polyvinyl butyral (PVB), polymethyl methacrylate, tetraethylenglycoldiacrylate) according to their functional subdivision [13–17]. Among binders described above, PEG has attracted more and more attention because of its non-toxic, harmless, and good water-soluble degreasing performance.

Various non-metallic and metal parts have been prepared in the application field by using binder PEG in the powder-forming method. For example, Kotz et al. prepared thermoplastic nanocomposites using the PEG+PVB system to realize high throughput injection molding and 3D printing of fused silica glasses with microstructures [3, 10]. In principle analysis, many studies of metal powder molding when PEG was a binder. For example, Thavanayagam et al. analyzed the rheological behavior of titanium feedstocks formulated with a water-soluble binder system for powder injection molding [18]. Hayat et al. analyzed the rheological properties and water-debinding behavior of Ti-MIM feedstocks from the perspective of PEG molecular weight [19]. Swan et al. studied the impact of PEG concentration on Titanium metal injection molding performance, and Taktak et al. studied the impact of PEG on sintered Alumina structure and mechanical properties [20].

However, there was a lack of in-depth discussion around theoretical or mechanical in the research field of fused silica glasses molding with binder PEG from non-metallic nano-silica powder. The interaction between PEG and nano-silica powder was more complex than that of metal powders because nano-silica has a higher specific

surface area when prepared nanocomposites were mixed with PEG. It was found that the molecular weight of PEG significantly influences the rheological and diffusion properties [19, 21–23], which will affect the performance of the final molding parts directly.

In order to prepare fused silica glass parts with suitable PEG molecular weight, the effects of PEG molecular weight on sintering silica glass from silica powder were studied.

2 Experimental

2.1 Materials

The experimental feedstocks are silica nanopowder of type Aerosil OX50 (with a mean diameter of ~ 40 and a surface area of $30\text{--}50 \text{ m}^2/\text{g}$) and binders of PEG (with different molecular weights of 200, 400, 800, 2000, 4000, 6000, 10,000 g/mol) and PVB (with a molecular weight in the range of 40,000–70,000 g/mol). All the materials are confined in The solvent of aqueous ethanol solution with 90 wt.%.

2.2 Producing feedstocks and analysis

Firstly, 15 wt.% PEG and PVB organic solution was prepared by using a laboratory dissolver stirrer to dissolve PEG and PVB in an aqueous ethanol solution with 90 wt %. Nano-silica suspension was prepared by dispersing silica nanopowder in an aqueous ethanol solution with 90 wt%. Then, two kinds of nanocomposite suspensions A and B were prepared by mixing organic solution and Nano-silica suspension. Nanocomposite suspension A: PEG organic solution + nano-silica suspension (silica of 10 vol%). Nanocomposite suspension B: PEG organic solution + PVB organic solution + nano-silica suspension (PEG, PVB with volume ratio of 1:1, silica of 56 vol%).

The viscosity of the PEG organic solution was analyzed by rheometer, and the pH of the PEG organic solution and the nano-silica suspension was measured. Nanocomposite suspension A was dried in a vacuum drying chamber at $75 \text{ }^\circ\text{C}$ for 36 h after pH analysis, then the simultaneous thermal analysis (differential scanning calorimeter, DSC+thermal gravimetric analysis, TGA) with nitrogen protection and heating rate of $10 \text{ }^\circ\text{C}/\text{min}$ from 30 to $1200 \text{ }^\circ\text{C}$ was conducted.

Nanocomposite suspension B was also dried in a vacuum drying chamber at $75 \text{ }^\circ\text{C}$ for 36 h and then the uniaxial molding was carried out by using a self-made hot pressing device with a mold cavity diameter of 20 mm [24]. Each time, nanocomposite suspension B of 1.2 g was pressed at a pressure of 5 tons and a temperature of $180 \text{ }^\circ\text{C}$ for 20 min, then it was taken out when cooled to $40 \text{ }^\circ\text{C}$. Pressed parts with dimensions of $20 \times \sim 2.5 \text{ mm}$ (diameter \times thickness) were finally obtained. Then the TGA with nitrogen

protection and heating rate of 10 °C/min from 30 to 800 °C was conducted for pressed parts.

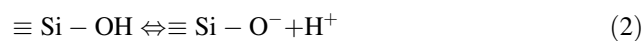
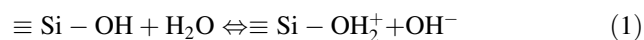
2.3 Debinding and sintering

The pressed green parts were debonded using a two-step process. First, the green parts were immersed in DI water at 40 °C for 4 h to remove the PEG component. After drying the partially debonded parts at 75 °C for 5 h, thermal debinding was performed in an ashing furnace with a heating rate of 1 °C/min and dwelling phases at the critical decomposition temperatures (270, 460, and 600 °C for 1 h each) in air. Vacuum sintering was done using a high-temperature tube furnace. The brown parts were sintered at 1300 °C for 30 min at a pressure of 1×10^{-2} mbar with heating and cooling rates of 3 °C/min, respectively. After sintering, the fused silica glasses were directly broken into two pieces by force, and then the section was blown clean by nitrogen with high pressure. The morphology of the section was observed by scanning electron microscope.

3 Results and discussion

3.1 Effect of PEG molecular weight on wet feedstocks performance

The pH test results are shown in Table 1. The pH of nano-silica suspension (SiO₂ only) is 6.65 due to the weak ionization h-ion reaction of silica in the solution. There were isolated free silanol groups (SiOH), linked silanol groups, and twin silanol groups on the surface of nano-silica powder (fumed silica) that have hydrophilic properties since formed hydrogen bonds with water molecular [22]. The conditions for silanol groups on SiO₂ particles in an aqueous solution are governed by the following surface equilibrium depending on the pH value [25]:



The SiO₂ suspension has an isoelectric point of pH = *pI* (*pI* < 7 usually). When the pH value of the SiO₂ suspension

is higher than *pI*, Eq. (2) shifts to the right. On the other hand, when the pH value of the SiO₂ suspension is lower than *pI*, Eq. (1) shifts to the right.

The pH values of PEG organic solution (PEG only) were all >7, and the pH was more significant with the increase of PEG molecular weight, such as the pH of PEG-200 was 7.64 while PEG-10,000 was 9.57. There were hydroxyl (hydrophilic, at both ends), methyl (hydrophobic, at both sides of the long chain), and an ether bond R-O-R' (in the middle) in a PEG molecule. Ether bonds provided two isolated pairs of electrons, and materials with such functional groups could be called Lewis bases according to Lewis acid-base theory [26]. The ether bond functional group has a weak external negative charge to combine H⁺ from water electrolysis, which increases the pH of the PEG organic solution. The solution pH increases with the increase of PEG molecular weight because PEG with higher molecular weight has a more significant number of ether bonds.

When PEG and silica powders are mixed into nanocomposite suspension A (hybrid), the pH of the hybrid will decrease compared with the PEG-only event of the same PEG molecular weight. Furthermore, the reason lies in the mutual adsorption (grafted reaction [27]) between the PEG molecules and the surface of SiO₂ powders [27–29], which caused the change in pH value. There was an artificial definition *f* used to show the strength of mutual adsorption:

$$f = \Delta pH = pH_{\text{peg-only}} - pH_{\text{hybrid}} \quad (3)$$

The changing trend of the strength of mutual adsorption *f* decreased firstly, then increased and decreased (ups and downs like fallen 'S' as shown in the red line in Fig. 3) with the decreasing PEG molecular weight. PEG-800 had a minimum *f* of 0.13, and PEG-6000 had a maximum *f* of 0.87. It meant that PEG-6000 could form the most robust binding with SiO₂ powders.

According to the study of Ikeda et al., the appropriate pH scope for silanol groups to be stable existence was around 2–3 [27]. The pH of the hybrid was not conducive to stabilizing silanol groups. The stratification phenomenon would appear in the nanocomposite suspension A after standing for 72 h (as shown in Fig. 1a) because the reduction of silanol groups weakened the steric hindrance effect

Table 1 Measured pH value at different PEG molecular weights

Projects	PEG-200	PEG-400	PEG-800	PEG-2000	PEG-4000	PEG-6000	PEG-10,000
SiO ₂ only	6.65						
PEG only	7.64	8.52	7.20	8.58	8.81	9.17	9.57
Hybrid	7.26	8.22	7.07	8.32	8.11	8.30	8.80
ΔpH	0.38	0.30	0.13	0.26	0.70	0.87	0.77

Bold values indicate statistical significance

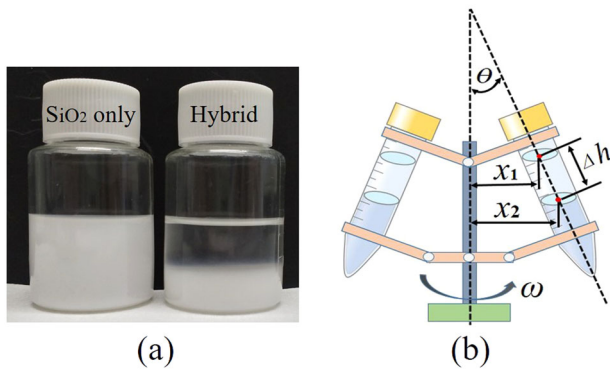


Fig. 1 **a** The optical image of nanocomposite suspension A after standing for 72 h. **b** Schematic diagram of flocculating particle radius r calculated by the centrifugal method

of the dispersed solute, and the silica nanoparticles collided with each other by Brownian motion to form flocculating particles [30].

In order to study the radius r of flocculating particles, Stokes settlement formula for spherical particles in liquid was introduced [31],

$$v = \frac{2r^2(\rho - \rho_0)g}{9\eta} \quad (4)$$

where v was the sedimentation velocity of the flocculating particle, r was the radius of the particle, ρ was the density of the particle, ρ_0 was the density of the medium, g was acceleration of gravity, and η was the viscosity of the medium.

The settlement formula was extended to the centrifugal field (as shown in Fig. 1b) and rewritten as:

$$\frac{4}{3}\pi r^3(\rho - \rho_0)\omega^2 x = 6\pi\eta r \frac{dx}{dt} \quad (5)$$

Here, x was the distance from the particle center to the axis rotation axis, centrifugal acceleration $\omega^2 x$ replaced gravitational acceleration g , integral solution of the above formula can be obtained:

$$6\pi\eta r \int_{x_1}^{x_2} \frac{dx}{x} = \frac{4}{3}\pi r^3(\rho - \rho_0)\omega^2 \int_{t_1}^{t_2} dt \quad (6)$$

The size of the flocculating particle was:

$$r = \sqrt{\frac{9}{2}\eta \times \frac{\ln(x_2/x_1)}{(\rho - \rho_0)\omega^2(t_2 - t_1)}} \quad (7)$$

x_1 and x_2 represent the distance from the liquid surface center to the rotation axis before and after centrifugation, θ was the tilt angle of the centrifugal tube ($\theta = 45^\circ$), Δh was the descending height of the liquid surface center, so

$$x_2 = x_1 + \Delta h \cdot \sin \theta \quad (8)$$

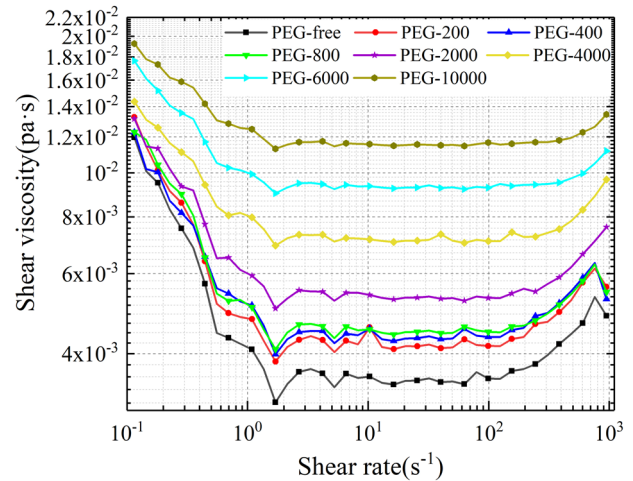


Fig. 2 Viscosity test results of PEG organic solutions with different molecular weights

Then, the final calculation form of flocculating particle size was:

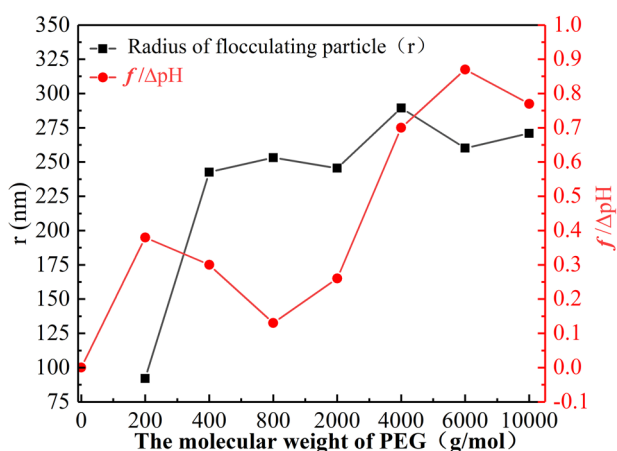
$$r = \sqrt{\frac{9}{2}\eta \times \frac{\ln(1 + \sqrt{2}\Delta h/2x_1)}{(\rho - \rho_0)\omega^2(t_2 - t_1)}} \quad (9)$$

The viscosity test results of the PEG organic solution were shown in Fig. 2. Overall, the viscosity decreases with increasing shear rates in the range of $0.1\text{--}1\text{ s}^{-1}$. In the range of shear rate from 1 to 100 s^{-1} , the shear viscosity basically keeps stable, and this stage was called the Newtonian fluid zone. When the shear rate is greater than 100 s^{-1} , the viscosity increases slightly because both of them tend to thicken at higher shear rates [32]. The average viscosity with a shear rate range of $1\text{--}100\text{ s}^{-1}$ was used as Eq. (9) to calculate the required viscosity parameters η .

The results of flocculating particle radius r and the parameters set in the experiment are listed in Tables 1 and 2. The changing trend of flocculating particle radius r and PEG-SiO₂ mutual adsorption strength f with PEG molecular weight increase were plotted in Fig. 3. It can be seen that the larger the PEG molecular weight was, the larger the flocculating particle radius r was. The corresponding trend of f was opposite to that of r with PEG molecular weight increase. The mutual adsorption strength f decreased when the particle radius r increased with the PEG molecular weight range of $200\text{--}800$ and $6000\text{--}10,000$. The change of mutual adsorption strength f reflected in the specific binding strength on the surface of PEG and nano-silica particles. The larger the binding strength was, the thicker the organic barrier film formed [22], which hindered the further agglomeration of nanoparticles. The final flocculating particle radius r was smaller. On the contrary, nano-silica particles tend to agglomerate together, and the agglomerated particle radius r was larger ($r \propto -f$).

Table 2 Parameters and results of particle radius calculation by Stokes sedimentation method

Parameters	PEG-200	PEG-400	PEG-800	PEG-2000	PEG-4000	PEG-6000	PEG-10,000
η (mPa·s)	4.20	4.36	4.47	5.31	7.11	9.27	11.53
ρ (g·cm ⁻³)				2.2			
ρ_0 (g·cm ⁻³)				1.019			
x_1 (cm)				10			
Δh (cm)	0.4	2.9	3.1	2.4	2.5	1.5	1.3
ω (rad·s ⁻¹)				133.33 π			
t_1 (s)				0			
t_2 (s)				30			
r (nm)	92	242	253	245	289	260	270

**Fig. 3** The curves of flocculating particle radius r and PEG-SiO₂ mutual adsorption strength f with increasing PEG molecular weight

3.2 Effect of PEG molecular weight on dry feedstocks performance

As shown in Fig. 4a, it can be seen that there were three upward exothermic peaks and one downward endothermic peak appearing in the DSC curve as the test temperature increased. They correspond to the events of energy storage release [28], oxidative decomposition, cold crystallization, and fusing thermal events, respectively. DSC test results shown in Fig. 4b indicate that the temperature at which the fusing thermal peak appeared first increases and then slightly decreases (the variation trend was marked by the block dotted arrow) with the increase of PEG molecular weight, which meant that the melting performance of nanocomposites changed with the increase of molecules. The shift in melting temperature point indicated the strength of the interactions between the PEG and SiO₂. For a more vital interaction between phase change materials SiO₂ and porous materials, the melting point will increase, while a weaker interaction will lead to a declined phase change temperature.

The change curve of specific heat capacity (drawn in Fig. 5b–i) of nanocomposite A with temperature increasing was obtained by analyzing and calculating the DSC test curves, and the specific heat capacity (C_p) and initial fusing temperature (T_i) of fusing thermal peaks were obtained from these curves (the extraction principle was shown in Fig. 5a). The particular explanation was that the sample C_p was on the negative Y-axis in Fig. 5b; this usually happened when the heat flow of the sample was lower than that of reference in the DSC instrument. To facilitate comparison, specific heat capacity (C_p) and initial fusing temperature (T_i) were plotted together with the previous curve of flocculating particle radius r changing with PEG molecular weight to Fig. 6.

In Fig. 6a, initial fusing temperature T_i and flocculating particle radius r showed a positive correlation with PEG molecular weight increase (except PEG-2000, if the trend was in the dotted line, the positive correlation could be fully satisfied). The events of PEG-200 and PEG-6000 have smaller particle radii r of ~92 and ~260 nm and relatively lower initial fusing temperature T_i of 873 and 934 °C, respectively. In Fig. 6b, the specific heat capacity C_p was positively correlated with the change of flocculating particle radius r with PEG molecular weight increase; the larger the radius r , the larger the specific heat capacity C_p . According to the Gibbs–Thomson equation (Eq. 10), the change in fusing temperature was macroscopically determined by the void size of composites. Meanwhile, the size of voids determines the strength of their energy storage, and the stronger the energy storage, the larger the specific heat capacity [33, 34].

$$\Delta T \propto \frac{1}{r - t} \quad (10)$$

In conclusion, the interaction between PEG and silica nanopowder could be divided into weak interaction (such as surface tension, capillary force, hydrogen bond, etc.) and intense interaction with grafted reaction [27] of silanol groups. The changes in the aggregated particles' flocculating particle radius r reflect these interactions'

Fig. 4 **a** Schematic diagram of TGA-DSC test curves analysis. **b** DSC test results of nanocomposite A

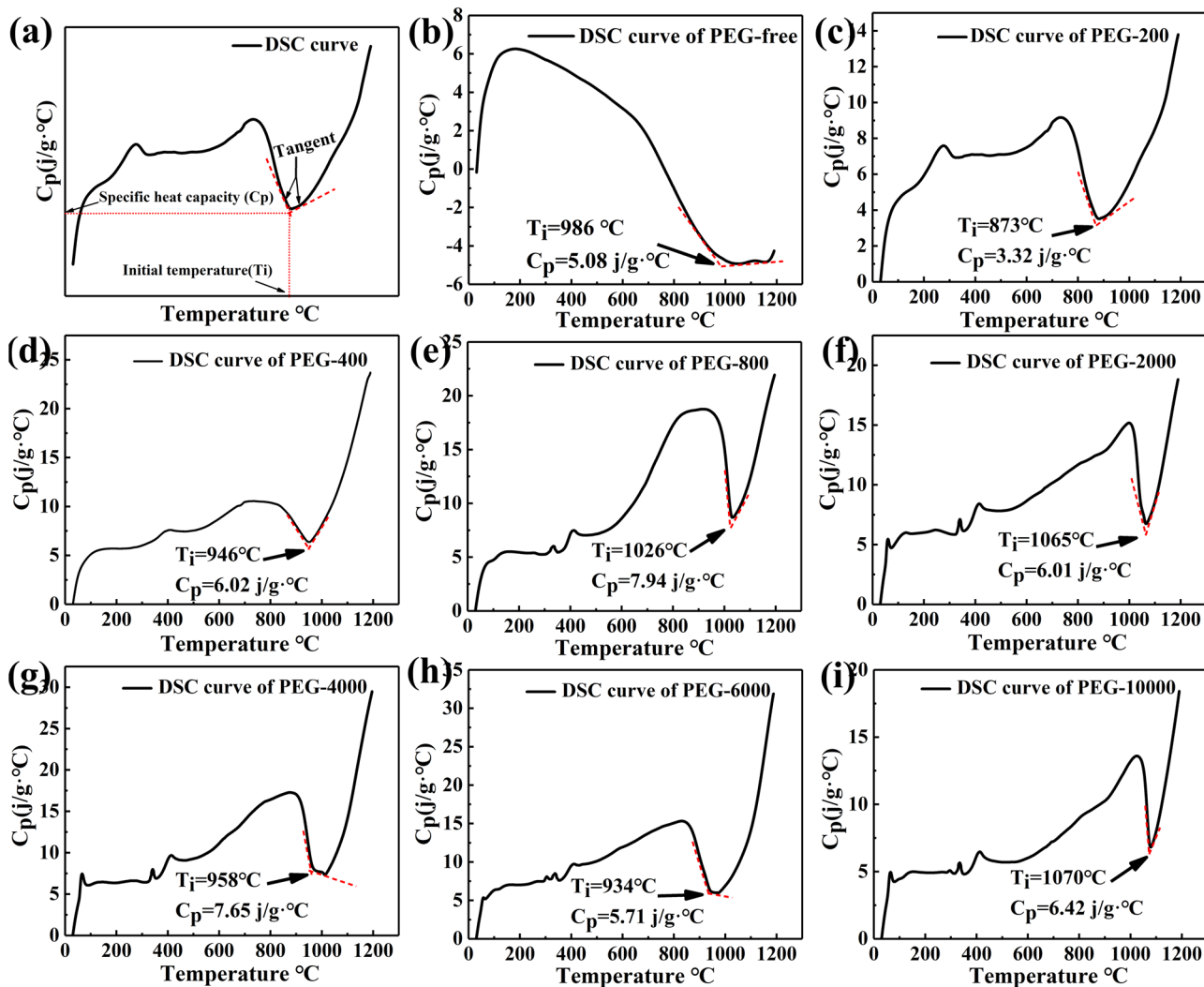
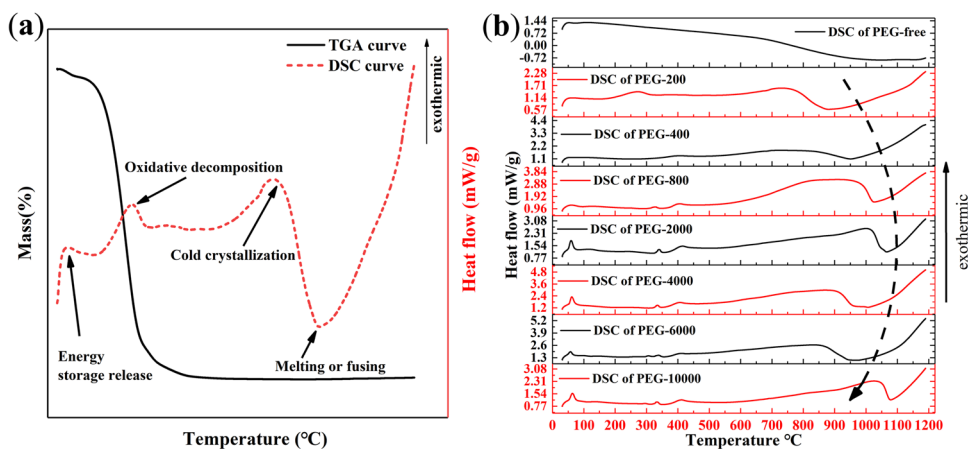


Fig. 5 Variation curves of specific heat capacity of nanocomposite A, **a** schematic diagram of specific heat capacity (C_p) and initial Fusing temperature (T_i) obtained, **b–i** specific test results curves of specific heat capacity with different PEG molecular weight

Fig. 6 Initial fusing temperature (T_i) (a), specific heat capacity (C_p) (b), and flocculating particle radius r as a function of PEG molecular weight

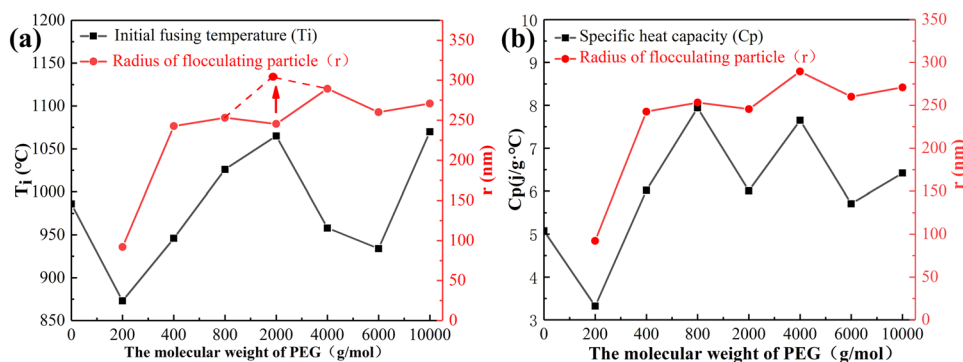
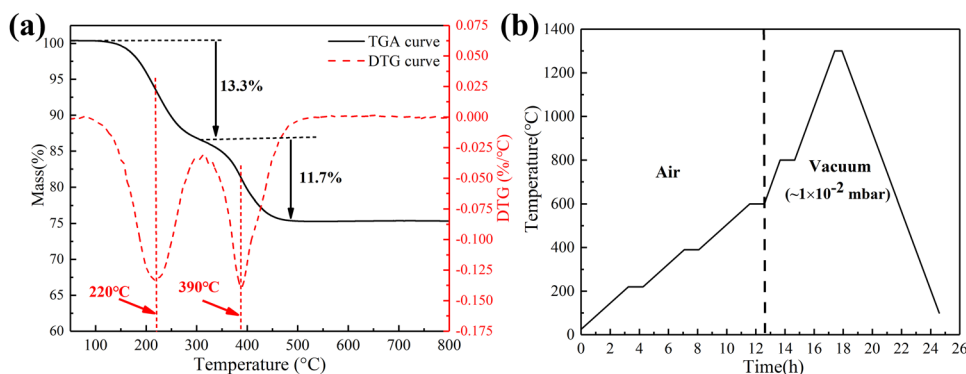


Fig. 7 a TG-DTG curves of pressed parts. b The temperature profile of debinding and sintering



overall effects. When the interaction between PEG and silica nanopowder was strong, the more substantial steric resistance effect of organic PEG made flocculating more challenging to occur. The flocculating particle radius r was smaller, which would lead to the dry feedstocks becoming more compact dry feedstocks with lesser voids, the initial fusing temperature T_i was reduced, and the specific heat capacity C_p was weaker. On the contrary, when the interaction was more vulnerable, the steric resistance effect of PEG was not noticeable, the flocculating particle radius r was more extensive, the dry feedstock with loose space was got, the fusing point T_i was higher, the energy storage was more robust, the specific heat capacity C_p was larger. Therefore, the initial fusing temperature T_i and specific heat capacity C_p of PEG-200 and PEG-6000 were lower.

3.3 Effect of PEG molecular weight on sintering properties

The TGA-DTG curves of the pressed parts are shown in Fig. 7a. The TGA curve indicates that there are two mass loss steps in the debinding process. It can be seen that there was a 13.3% mass loss at 100–310 °C, mainly caused by the oxidative decomposition of the polymers PEG and PVB. Mass loss from 310 to 520 °C was 11.7% due to the further removal of incomplete oxidized carbonyl groups from the

pressed parts. Finally, the remaining mass was 75%. The temperature distribution of debinding and sintering was shown in Fig. 7b according to the obtained results of the differential thermal gravity analysis. DTG curve showed that there were two mass loss rate peaks at 220 and 390 °C, respectively. Then, the heat preservation stages of 220, 390, and 600 °C were set with a heating rate of 1 °C/min and a holding time at each stage of 1 h. The purpose of 600 °C heat preservation was to remove the organic residue thoroughly. The heat preservation at 800 °C during the sintering process was to reduce the hydroxyl content in the debinding parts. Finally, the parts were sintered at 1300 °C for 30 min at a pressure of 1×10^{-2} mbar with heating and cooling rates of 3 °C/min, respectively. Eventually, the whole heat treatment time was ~ 24.5 h.

Figure 8 shows the nanocomposite results using uniaxial molding with different PEG molecular weights. In Fig. 8a, the bonding performance between particles was poor, and the regular circular part was difficult to form because there was no PEG, and only the binder PVB existed. Figure 8b–d shows better-pressing results and the more minor crack defect in the side view with the increase of PEG molecular weight because PEG was liquid or thick at room temperature and had limited bonding performance when PEG molecular weight was from 200 to 800, while Fig. 8e–h shows that PEG-2000–10,000 was ideal pressed and can be formed as a complete green part.

Fig. 8 Front and side optical images of nanocomposite B after pressing. **a–h** PEG-free, PEG-200, PEG-400, PEG-800, PEG-2000, PEG-4000, PEG-6000, and PEG-10,000, respectively

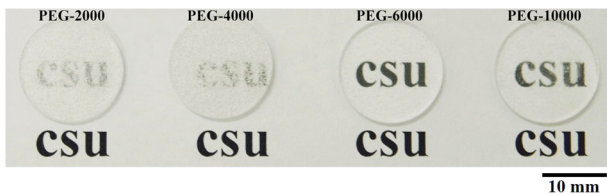
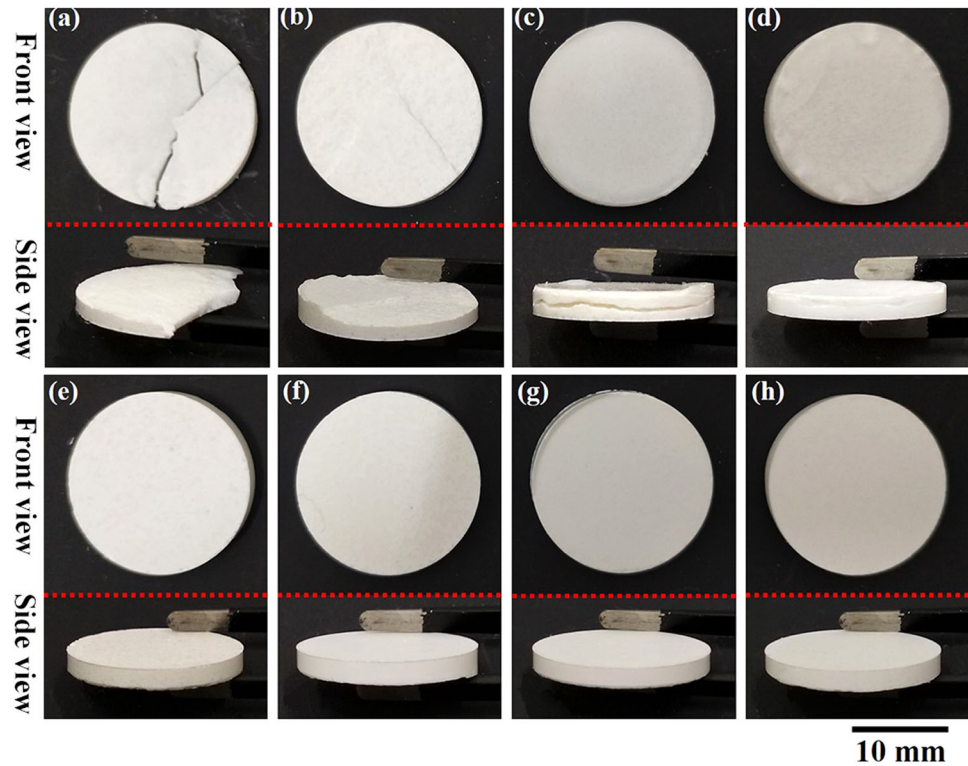


Fig. 9 The optical images of pressed parts after sintering with PEG molecular weights of 2000, 4000, 6000, and 10,000

After two-step degreasing and vacuum hot sintering the green parts containing PEG-2000~10,000, the results are shown in Figs. 9 and 10.

The sintering results shown in Fig. 9 indicated that the fused silica glasses with the best optical quality could be obtained using a binder of PEG-6000, while the visual quality with PEG-2000, 4000, and 10,000 was dissatisfactory. As shown in Fig. 10, the number and size of seam defects directly affect the final optical quality. There was no internal defect (as shown in Fig. 10b), and the optical quality was best with the PEG-6000.

Interestingly, the quality of sintered fused silica glasses is similar to the initial fusing temperature T_i in the thermal analysis experiment. As shown in Fig. 11, in the region of uniaxial pressing molding successfully, the sintered glass quality increases as the initial fusing temperature T_i decreases and then decreases as the T_i increases, where the best optical quality was obtained at the lowest fusing point (PEG-6000) since the strength of mutual adsorption f lead to smaller flocculating

particle radius r and lower initial fusing temperature T_i , the final sintered products shown better optical quality with less or noninternal defects.

4 Conclusions

The effect of binder PEG with different molecular weights on fused silica glasses sintering using silica nanopowder was studied. The following conclusions can be drawn:

1. The pH tests and centrifugal sedimentation results indicated a negative correlation between flocculating particle radius r and the strength of mutual adsorption f with PEG molecular weight increased ($r \propto -f$).
2. The initial fusing temperature T_i and specific heat capacity C_p were positively correlated with the size of the flocculating particle radius r with the PEG molecular weight increased ($T_i \& C_p \propto r$).
3. The sintered part with PEG-6000 can be completely densified with good optical quality and non-seam defects because the initial fusing temperature T_i and specific heat capacity C_p were minimal. In other words, the transparent fused silica glasses were decided by the flocculating particle radius r , the strength of mutual adsorption f , the initial fusing temperature T_i and specific heat capacity C_p , and there was a loose relation of $T_i \& C_p \propto -r \propto f$.

Fig. 10 The cross-sectional SEM images of the silica pellets were sintered with different PEG molecular weights of **a** 2000, **b** 4000, **c** 6000, and **d** 10,000. Sintering time of 30 min

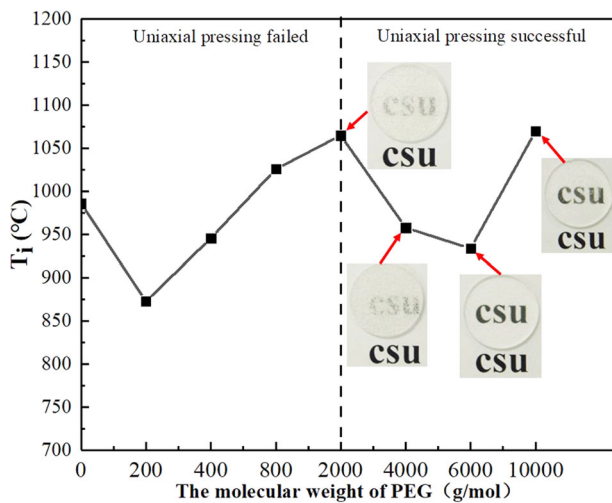
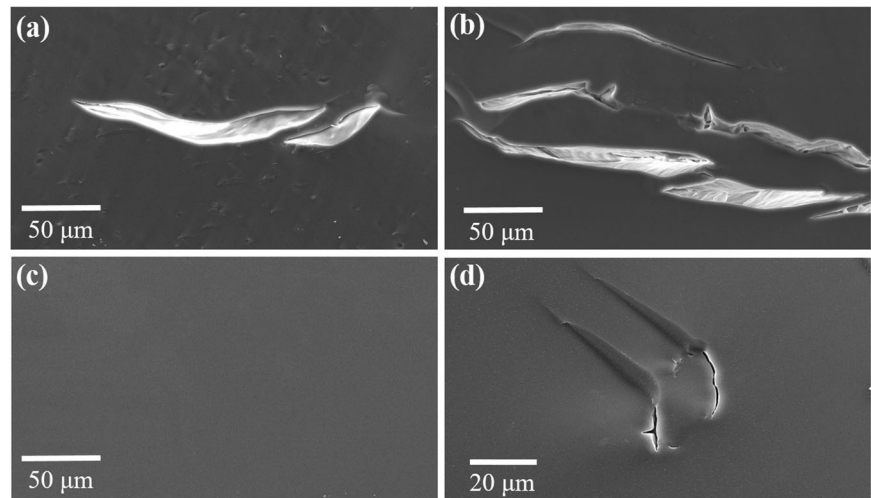


Fig. 11 The curve of initial fusing temperature T_i and sintering quality

Acknowledgements This work was supported by the National Natural Science Foundation of China (51875585, 51875584, and 51935013) and the Opening Project of Science and Technology on Reliability Physics and Application Technology of Electronic Component Laboratory (ZHD202001). We are very grateful to Professor Fuliang Wang for his support to this work in valuable suggestions.

Compliance with ethical standards

Conflict of interest The authors declare no competing interests.

References

- Lin Z, Xinpeng Z, Chengwei W et al. (2022) Rapid pressureless sintering of glasses. *Small* 18:e2107951
- Lin D, Seungryeol Y, Jong H et al. (2015) Fabrication of glass components by sintering of commercial glass powder. *Ceram Int* 41(3):5057–5065
- Mader M, Schlatter O, Heck B et al. (2021) High-throughput injection molding of transparent fused silica glass. *Science* 372(6538):182–186
- Kotz F, Norbert S, Andreas S et al. (2018) Glassomer-processing fused silica glass like a polymer. *Adv Mater* 30(22):1707100
- Shackelford J-F (1999) Gas solubility in glasses – principles and structural implications. *J Non Cryst Solids* 253(1):231–241
- Monk D-J, Soane D-S, Howe R-T (1993) A review of the chemical reaction mechanism and kinetics for hydrofluoric acid etching of silicon dioxide for surface micromachining applications. *Thin Solid Films* 232(1):1–12
- Chen YH, Xing H, Tong L et al. (2021) Obtaining transparent silica glass from nano-silica hydrosol. *Ceram Int* 47(14):19340–19345
- Nakane K, Tomonori Y, Kenji I et al. (1999) Properties and structure of poly(vinyl alcohol)/silica composites. *J Appl Polym Sci* 74(1):133–138
- Rabinovich E-M (1985) Preparation of glass by sintering. *J Mater Sci* 20(12):4259–4297
- Mader M, Leonhard H, Phillip S et al. (2021) Melt-extrusion-based additive manufacturing of transparent fused silica glass. *Adv Sci* 8(23):2103180
- Wen X, Boyu Z, Weipeng W et al. (2021) 3D-printed silica with nanoscale resolution. *Nat Mater* 20(11):1506–1511
- Xu Y, Ye L, Ning Z et al. (2021) Transparent origami glass. *Nat Commun* 12:1
- Tong Y-H, Liu Y-C, Lu S-X et al. (2004) The optical properties of ZnO nanoparticles capped with polyvinyl butyral. *J Sol-gel Sci Technol* 30(3):157–161
- Veselov S, Cherkasova N, Kuzmin R et al. (2017) Microstructure and properties of 3Y-TZP ceramic fabricated using PEG temporary binder. *IOP Conf Ser Mater Sci Eng* 286(1):12022
- Hayat M-D, Aparajita G, Steven M et al. (2017) Modification of PEG/PMMA binder by PVP for titanium metal injection moulding. *Powder Technol* 315:243–249
- Feng Y, Kun W, Jianfeng Y et al. (2013) Effect of the addition of polyvinylpyrrolidone as a pore-former on microstructure and mechanical strength of porous alumina ceramics. *Ceram Int* 39(7):7551–7556
- Kotz F, Klaus P, Werner B et al. (2016) Liquid glass: a facile soft replication method for structuring glass. *Adv Mater* 28(23):4646–4650
- Thavanayagam G, Pickering K-L, Swan J-E et al. (2015) Analysis of rheological behaviour of titanium feedstocks formulated with a

- water-soluble binder system for powder injection moulding. *Powder Technol* 269:227–232
19. Hayat M-D, Guian W, Mohd-Fikri Z et al. (2015) Effect of PEG molecular weight on rheological properties of Ti-MIM feedstocks and water debinding behaviour. *Powder Technol* 270:296–301
 20. Thavanayagam G, Swan J-E (2018) Aqueous debinding of polyvinyl butyral based binder system for titanium metal injection moulding. *Powder Technol* 326:402–410
 21. Shimada K, Haruhisa K, Takeshi S et al. (2005) Precise measurement of the self-diffusion coefficient for poly(ethylene glycol) in aqueous solution using uniform oligomers. *J Chem Phys* 122(24):244914
 22. Raghavan S-R, Walls H-J, Khan S-A (2000) Rheology of silica dispersions in organic liquids: new evidence for solvation forces dictated by hydrogen bonding. *Langmuir* 16(21):7920–7930
 23. Wang F, Kang Z, Qinglong Z et al. (2019) Effect of molecular weight and concentration of polyethylene glycol on through-silicon via filling by copper. *Microelectron Eng* 2019(215):111003
 24. Wang F, Nantian N, Hu H et al. (2017) Ultrasonic-assisted sintering of silver nanoparticles for flexible electronics. *J Phys Chem C* 121(51):28515–28519
 25. Ikeda H, Fujino S, Kajiwara T (2011) Preparation of SiO₂-PVA nanocomposite and monolithic transparent silica glass by sintering. *J Ceram Soc Jpn* 119(1385):65–69
 26. Grabowski S-J (2020) Hydrogen bond and other Lewis Acid-Lewis Base interactions as preliminary stages of chemical reactions. *Molecules* 25(20):4668
 27. Lin B, Zhou S (2017) Poly(ethylene glycol)-grafted silica nanoparticles for highly hydrophilic acrylic-based polyurethane coatings. *Prog Org Coat* 106:145–154
 28. Li J, Lihong H, Tangzhi L et al. (2013) Preparation and characterization of PEG/SiO₂ composites as shape-stabilized phase change materials for thermal energy storage. *Sol Energy Mater Sol Cells* 118:48–53
 29. Wang C, Lili F, Wei L et al. (2012) Shape-stabilized phase change materials based on polyethylene glycol/porous carbon composite: the influence of the pore structure of the carbon materials. *Sol Energy Mater Sol Cells* 105:21–26
 30. Ikeda H, Shigeru F (2014) Composition and pH dependence on aggregation of SiO₂-PVA suspension for the synthesis of porous SiO₂-PVA nanocomposite. *J Porous Mater* 21(6):1143–1149
 31. Richardson J-F, Zaki W-N (1997) Sedimentation and fluidisation: part I. *Chem Eng Res Des* 75:S82–S100
 32. Liu X-Q, Rui-Ying B, Xiao-Jun W et al. (2015) Temperature induced gelation transition of a fumed silica/PEG shear thickening fluid. *RSC Adv* 5(24):18367–18374
 33. Zhang D, Zhou J, Keru W et al. (2005) Granular phase changing composites for thermal energy storage. *Sol Energy* 78(3):471–480
 34. Findenegg G-H, Susanne J, Dilek A et al. (2008) Freezing and melting of water confined in silica nanopores. *ChemPhysChem* 9(18):2651–2659

Publisher's note Springer Nature remains neutral with regard to jurisdictional claims in published maps and institutional affiliations.

Springer Nature or its licensor (e.g. a society or other partner) holds exclusive rights to this article under a publishing agreement with the author(s) or other rightsholder(s); author self-archiving of the accepted manuscript version of this article is solely governed by the terms of such publishing agreement and applicable law.